Research Square

Preprints are preliminary reports that have not undergone peer review.
They should not be considered conclusive, used to inform clinical practice,
or referenced by the media as validated information.

Thermal Behaviour and Household-Energy Implications of Rice-Husk–Palm-Kernel-Shell Blends

Umaru Ahmadu
Federal University of Technology
Halilu Jume Ibrahim
Federal University of Technology
Yakubu A. Bala
Federal Polytechnic Bida
Abubakar Sadiq Yusuf
sadiq.yusuf@vuw.ac.nz
Victoria University of Wellington
Moses Agida
Federal University of Technology
Bello Abdulkadir
Federal University of Technology

Research Article

Keywords: briquettes, rice husk, palm kernel shell, proximate analysis and physico-chemical characterisation

Posted Date: November 10th, 2026

DOI: https://doi.org/10.21203/rs.3.rs-11419244/v1

License: This work is licensed under a Creative Commons Attribution 4.0 International License.
Read Full License

Additional Declarations: No competing interests reported.

THERMAL BEHAVIOUR AND HOUSEHOLD-ENERGY IMPLICATIONS OF RICE-HUSK–PALM-KERNEL-SHELL BLENDS

U. Ahmadu[1]*, Halilu Ibrahim J.[1], Bala Yakubu A.[1,2,5], Abubakar Sadiq, Y. [1, 3], Moses Agida[1], Bello Abdulkadir[4]

[1] School of Physical Sciences, Department of Physics, Federal University of Technology, PMB 65, Minna, Niger State, Nigeria.*

[2]Department of Physics, Federal Polytechnic Bida, Nigeria.

[3]School of Engineering, Computer and Mathematical Sciences, Auckland University of Technology, PO Box 92006, Auckland 1142, New Zealand.

[4]Department of Mechanical Engineering, Federal University of Technology, Minna, Nigeria.

[5]Robinson Research Institute, Victoria University of Wellington, PO Box 33436, Petone 5046, New Zealand

[*]**Corresponding authors**: umaruahmadu@futminna.edu.ng, Sadiq.yusuf@vuw.ac.nz

Abstract

Agricultural residues such as rice husk (RH) and palm kernel shell (PKS) are abundant, low-cost biomass wastes that can be valorised into briquettes as a sustainable alternative to conventional solid fuels. This study investigated the physico-chemical and thermal properties of briquettes produced from RH and PKS powders blended at RH: PKS weight ratios of 100:0, 90:10 (A), 80:20 (B), 70:30 (C), 60:40 (D), 50:50 (E) and 0:100, with structural and thermal characterisation performed using XRD, FTIR, SEM-EDX, TGA/DTG and DSC. Proximate analysis gave moisture, ash, volatile matter and fixed carbon contents of up to 5.57%, 19.32%, 81.38% and 2.11%, respectively, for the briquettes, with fixed carbon calculated by difference. Compositional analysis showed that RH contained a higher cellulose content (18.24%) than PKS (15.91%), in addition to having more hemicellulose (29.82%) than PKS (17.44%), while PKS was markedly richer in lignin (58.72% against 30.06%). Ultimate analysis indicated carbon, hydrogen, oxygen, nitrogen and sulfur contents ranging from 28.86-43.62%, 13.58-29.25%, 28.79-47.83%, 0.56-1.06% and 0.80-1.08%, respectively. Sample E (50:50) exhibited the highest experimental higher heating value (19.19 MJ/kg), which was 18% above the value predicted from proximate data (15.65 MJ/kg). XRD showed a broad amorphous halo centred near $2\theta = 22°$ in all samples, whereas FTIR confirmed cellulose-, hemicellulose- and lignin-related functional groups, together with silica-related bands in RH. TGA/DTG showed that RH-rich samples decompose at lower temperature than PKS-rich blends. Overall, the findings demonstrate that the optimal RH: PKS blend ratio is property-dependent, providing guidance for tailoring briquette composition to specific fuel applications.

Keywords: *briquettes, rice husk, palm kernel shell, proximate analysis and physico-chemical characterisation.*

1. Introduction

The global drive toward sustainable development has intensified interest in diversifying energy supply away from fossil fuels toward renewable alternatives capable of reducing carbon emissions. Household energy use accounts for a substantial share of total energy consumption in developing countries, where cooking alone represents a major component of domestic demand, and where many rural households and a considerable proportion of urban households still rely on solid biomass fuels for heating and cooking (WHO, 2025). Millions of tonnes of agricultural residues are generated worldwide each year; where these residues are not recovered, they are frequently disposed of by open burning, contributing to air pollution and greenhouse gas emissions. Densifying such residues into high-density fuel briquettes offers a practical route for converting agricultural waste into a renewable energy carrier (Jume et al., 2024), and briquettes have gained growing acceptance globally as a substitute for fuelwood and charcoal in domestic, commercial and light-industrial heating applications (Lichinga et al., 2025).

Nearly one-third of the global population, an estimated 2.1 billion people, still cook using open fires or inefficient stoves fuelled by kerosene, biomass or coal. Combustion of these fuels indoors releases high concentrations of carbon monoxide, nitrogen and sulphur oxides, and particulate matter; household air pollution was responsible for an estimated 2.9 million premature deaths in 2021 alone, including more than 300,000 deaths of children under five (WHO, 2025). Sub-Saharan Africa remains the region where population growth continues to outpace progress on clean cooking access, with roughly 923 million people still lacking access as of 2022 (WHO, 2025). Concerns over the eventual depletion of fossil resources add further urgency to the search for sustainable alternative energy sources, in line with the emissions-reduction commitments of the 2015 Paris Agreement (United Nations, 2015a) and Sustainable Development Goal 7 on affordable and clean energy for all (United Nations, 2015b).

In Nigeria specifically, energy poverty, driven by rising demand, an unreliable national grid, and escalating costs of electricity and liquefied petroleum gas (LPG), remains a pressing concern. According to the National Bureau of Statistics' most recent residential energy survey, about 67.8% of Nigerian households still rely on fuelwood as an energy source (NBS, 2024), a dependence that has contributed to severe forest loss: Nigeria is estimated to have lost close

to 90% of its original forest cover over the past three decades, and is among the fastest rates of deforestation recorded globally (NCF, 2026). Reversing this trend requires viable, locally sourced alternatives to fuelwood and charcoal.

Rice husk (RH) and palm kernel shell (PKS) are among the most abundant agricultural residues generated across Nigeria. Rice husk is a lignocellulosic waste material typically containing 20-22% silica-rich ash together with cellulose, hemicellulose and lignin fractions; its comparatively high ash content and low bulk density have historically limited its direct use as a solid fuel (Vui et al., 2025). Palm kernel shell, the hard endocarp surrounding the oil palm kernel (Elaeis guineensis) and a major by-product of palm oil extraction, is by contrast rich in fixed carbon and lignin, exhibits low ash and moisture content, and possesses a high calorific value, properties that make it attractive for direct combustion and for densification into briquettes (Tarigan et al., 2026).

Blending residues with complementary properties, such as RH and PKS, has been shown to improve the calorific value and combustion behaviour of the resulting briquettes relative to single-feedstock briquettes (Jume et al., 2024; Tarigan et al., 2026). However, the combined use of RH and PKS across a range of blend ratios, and the way blending changes the chemical composition, structure and thermal decomposition of the fuel, remains comparatively underexplored. Because these properties determine ignition, burning rate and heat release in a cookstove, they are the basis on which a blend should be chosen. This study therefore blended RH and PKS at seven weight ratios and linked, step by step, (i) the proximate, elemental composition of the feedstocks and briquettes, (ii) their experimental and theoretically estimated heating values, (iii) their crystalline/amorphous structure, functional groups and morphology, and (iv) their thermal decomposition behaviour, with the aim of identifying the blend compositions offering the best combination of fuel and thermal properties for cost-effective cooking and heating. The findings are intended to provide practical guidance for formulating RH-PKS briquettes in regions where either raw material may be scarce, seasonally limited or costly, while still achieving competitive calorific value.

2. Materials and Methods

2.1 Materials

2.1.1 Collection and preparation of biomass feedstocks

Rice husk (RH) and palm kernel shell (PKS), locally available agricultural residues in Nigeria, were selected as the biomass feedstocks. RH was obtained from rice-milling facilities in Bida

and Kontagora along the Minna-Rijau Road corridor, Niger State, Nigeria. PKS was obtained from the Etsu Yahaya Oil Mill in Bida (3 km along Minna Road), Niger State, Nigeria. Cassava starch was used as the binder. All samples were transported to the NRF2021 Laboratory (Biomass Briquetting and Cookstove Testing), Department of Physics, Federal University of Technology, Minna (FUT Minna), where stones, dust, metal debris and extraneous plant matter were removed manually and the cleaned residues were sun-dried in ambient air for 48 h. The dried residues were pulverised in a 5-hp electrical grinding machine at the Central Workshop, Department of Mechanical Engineering, FUT Minna (repeated passes over 2 h for RH and 4 h for PKS, until a particle size of about 1.5 mm was reached), sun-dried for a further 72 h at ambient temperature and stored in sealed low-humidity polyethylene sacks until densification. The overall preparation and characterisation sequence is presented in Figure 1. Before briquetting, the ground feedstocks were sieved to a uniform particle size of 1 mm and thoroughly mixed to obtain homogeneous formulations. The same 1 mm powders (or, for briquettes, 1 mm powders obtained by crushing and sieving the dried briquettes) were used for all characterisation tests described below.

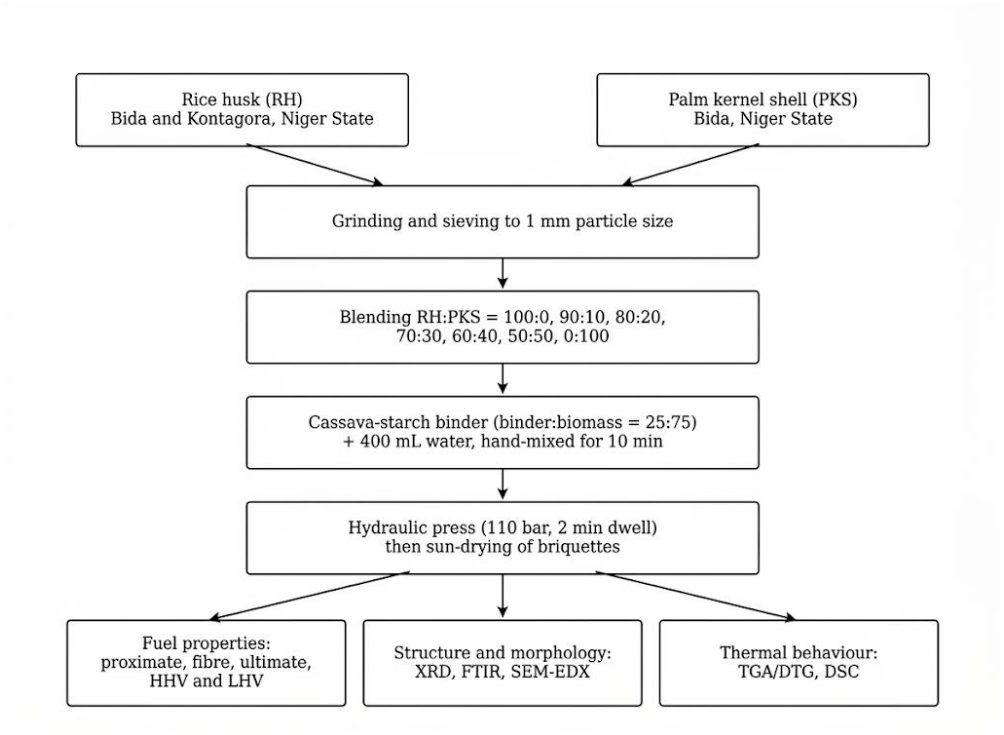


Figure 1. Preparation and characterisation sequence for the RH-PKS briquettes.

2.1.2 Preparation of cassava-starch binder

One litre of water was brought to boiling in a pot using a local charcoal stove. Separately, 400 g cassava starch was dispersed in 0.5 L cold water to form a smooth paste. The paste was

gradually introduced into the boiling water with continuous stirring for approximately 15-20 min until a thick, cloudy gel was formed. The gel was allowed to cool to room temperature for 2-3 h before use. The binder was incorporated at a binder-to-biomass ratio of 25:75.

2.2 Experimental production of briquettes

Briquettes were produced in the TETFUND NRF 2021 Laboratory (Biomass Briquetting and Cookstove Testing), Department of Physics, Federal University of Technology, Minna, Nigeria, using the NRF2021 briquetting machine. RH and PKS were prepared at seven mass ratios (RH: PKS): 100:0 (RH), 90:10 (A), 80:20 (B), 70:30 (C), 60:40 (D), 50:50 (E) and 0:100 (PKS). The formulations are listed in Table 1. The cassava-starch binder was added at 25% of the briquette mass (binder: biomass = 25:75). A total of 400 mL water was used during mixing, and the biomass, binder and water were manually mixed for 10 min.

Each formulation was hand-fed into the mould and compacted with a manually operated 20-tonne hydraulic piston press at 110 bars. Compaction was performed at approximately 35 °C and 25% relative humidity, with a 2-min dwell time after loading to minimise spring-back. The biomass was compacted in cylindrical steel moulds of 50 mm internal diameter. Twelve briquettes were produced per batch; the production capacity was 12 briquettes per 18 min. The briquettes were cylindrical and contained a central 1.0-cm-diameter hole intended to increase porosity and facilitate air supply during combustion (Figure 2). The briquettes were then sun-dried for approximately 31 days to constant mass before characterisation. Drying was carried out in a well-ventilated outdoor environment under ambient atmospheric conditions.



Figure 2. The sample of fuel briquettes produced from rice husk and palm kernel shell

Table 1: Blending ratios of biomass samples with 25 % cassava starch gel binder.

Sample ID	RH (wt.%)	PKS (wt.%)	Classification of Single/Blends
RH	100	0	Raw
PKS	0	100	Raw
A	90	10	Binary
B	80	20	Binary
C	70	30	Binary
D	60	40	Binary
E	50	50	Binary

2.3 Proximate analysis

Moisture content (MC), volatile matter (VM), ash content (AC) and fixed carbon (FC) were determined on the RH and PKS powders and on the composite samples (particle size 1 mm). Each property was measured once on one test portion per sample; no replicate determinations were used, so the values reported are single results. All determinations were carried out in a laboratory atmosphere (about 35 °C and 25% relative humidity, ambient air), and masses were recorded with an analytical balance (0.0001 g readability). The following procedures, based on ASTM D3173 (moisture), ASTM D3175 (volatile matter) and ASTM D3174 (ash) with fixed carbon obtained by difference as defined in ASTM D3172, were used.

2.3.1 Moisture Content

A 1.0 g sample of powdered biomass was placed in a pre-weighed aluminium dish and dried in an oven at 105°C for 1 h. The dish was then cooled in a desiccator and re-weighed according to ASTM D3173. Moisture content was calculated using Equation (1):

$$\text{Moisture Content (\%MC)} = \frac{W_1 - W_3}{W_2 - W_1} \times 100\ \% \qquad (1),$$

where, W_1 is the weight of the empty dish, W_2 is the weight of the dish and sample prior to oven drying, and W_3 is the weight of the dish and sample after oven drying.

2.3.2 Volatile Matter

A 1.0 g sample was weighed into a pre-weighed, lidded crucible and combusted in a muffle furnace according to ASTM D3175 for particulate wood fuels. The sample was held at 105°C and subsequently heated to 950°C for 7 min. The crucible was then removed, cooled in a desiccator, and re-weighed. Volatile matter content was calculated using Equation (2):

$$\text{Volatile Matter (\%VM)} = \frac{W_2 - W_3}{W_2} \times 100\ \% \qquad (2),$$

where W_2 is the sample mass after drying at 105◦C, and W_3 is the sample mass remaining after heating at 950◦C.

Ash content was determined according to ASTM D3174. A 1.0 g sample was placed into a pre-weighed crucible and ignited in a muffle furnace at 760∘C until complete ash formation (white or light grey residue) was observed. After cooling in a desiccator, ash content was calculated using Equation (3):

$$\text{Ash Content (\%)} = \frac{W_3 - W_2}{W_2 - W_1} \times 100\ \% \qquad (3)$$

where W_1 is the weight of the empty crucible, W_2 is the weight of the crucible and sample prior to incineration, and W_3 is the weight of the crucible and ash residue following combustion.

2.3.4 Fixed Carbon

The percentage of fixed carbon was calculated by difference using Equation (4):

$$\text{Fixed Carbon (\%FC)} = 100 - (\%MC + \%VM + \%AC) \qquad (4)$$

2.4 Structural/Compositional Analysis

The structural components (cellulose, hemicellulose, and lignin) of the biomass samples were quantified using standard sequential extraction techniques based on AOAC Method 973.18.

2.4.1 Acid Detergent Fiber (ADF) and Acid Detergent Lignin (ADL)

Acid detergent fiber (ADF) was determined via filtration. A 1.0 g sample (W_1) was placed in a pre-weighed fritted crucible, defatted using acetone, and boiled sequentially in an acid detergent solution (ADS) for 60 min. The residue was dried in an oven at 130◦C for 2 h, cooled in a desiccator, and weighed (W_2). To determine ADL, 25 mL of 72% H_2SO_4 was added to the residue in the crucible and allowed to react for 3 h with hourly stirring. The acid was filtered out, and the sample was washed with deionized water until free of acid. The crucible was dried at 130∘C for 2 h, cooled, and weighed (W_4). The sample was then ashed at 525±15◦C for 3 h, cooled, and re-weighed (W_5). The percentages of ADF, ADL, and cellulose were calculated using Equations (5) and (6):

$$\%\ \text{ADF} = \frac{W_2 - (W_3 + C)}{W1} \text{ x } 100 \qquad (5)$$

$$\% \text{ ADL} = \frac{W_4-(W_5+C)}{W1} \text{ x } 100 \quad (6),$$

where W_1 is the initial sample mass, W_2 is the dry crucible and residue weight after ADS extraction, W_3 is the empty crucible weight, W_4 is the crucible and residue mass post-acid treatment, W_5 is the crucible and ash residue weight post-ignition, and C is the blank correction factor.

2.4.2 Neutral Detergent Fiber (NDF)

Neutral detergent fiber (NDF) was quantified using a filtration technique. Approximately 1.00 g of Celite filter aid was added to a pre-dried crucible (W_1), followed by 0.50 g of sample. After defatting with 25 mL of acetone, the sample was rinsed with water. To prevent foaming, 50 mL of cold Neutral Detergent Solution (NDS) and 0.5 g of Na_2SO_3 were added. The mixture was refluxed for 30 min, washed thoroughly with hot deionized water, and dried in an oven at 130±2°C for 2 h. The crucible was cooled to room temperature in a desiccator and weighed (W_2). After ashing at 520±25°C for 3 h, the crucible was cooled and weighed (W_3). NDF and hemicellulose contents were computed using Equation (7):

$$\% \text{ NDF} = \frac{W_2-W_3+\text{blank})}{W1} \text{ x } 100 \quad (7)$$

$$\% \text{ Hemicellulose} = \%\text{NDF} - \%\text{ADF} \quad (8)$$

2.5 Ultimate Analysis

The elemental composition (C, H, N, S, and O) of powdered briquette samples was measured using a HACH Model DR/2010 LE 811 Series CHNSO elemental analyser. Test specimens (3–4 mg, particle size ≤1 mm) were encapsulated in tin foil and introduced into the analyser's combustion chamber. Gaseous combustion products (CO_2, H_2O vapor, and N_2) were separated chromatographically and quantified using a thermal conductivity detector (TCD). Measurements were calibrated using reference standards in accordance with ASTM E777-08 and ASTM E778-08, including 2,5-bis (5-tert-butyl-2-benzoxazol-2-yl) thiophene (BBOT) and oatmeal. Oxygen content was determined by difference using Equation (9):

$$\text{Oxygen (\%)} = 100 - (\%\text{C} + \%\text{H} + \%\text{N} + \%\text{S} + \%\text{Ash}) \quad (9)$$

2.6 Experimental and theoretical heating values

The experimental higher heating value (HHV) was determined on the 1 mm samples with an XRY-1A oxygen bomb calorimeter (National Centre for Energy Research and Development, University of Nigeria, Nsukka) following ASTM D5865/D5865M (ASTM International,

2019). About 0.5 g of sample, weighed to 0.0001 g, was placed in the crucible in contact with a 10 cm ignition wire and a cotton thread. The bomb was charged with 10 mL of distilled water, filled with pure oxygen to 2.8-3.0 MPa and immersed in the water jacket in ambient laboratory air. The initial water temperature was recorded after 2 min of continuous stirring and the final temperature at 31 min. Unburned wire was measured and the bomb washings were titrated with 0.0709 N sodium carbonate solution (methyl red indicator) to correct for nitric and sulfuric acid formation. The temperature rise was corrected for heat exchange, and the energy equivalent of the calorimeter was established by calibration with benzoic acid. The bomb calorimeter gives the gross (constant-volume) value, so the lower heating value (LHV) cannot be measured directly and was obtained by correcting the experimental HHV for the water formed from hydrogen (Equation 11).

Theoretical HHV was estimated from the proximate data with the correlation of Qian et al. (2020), in which VM and FC are in wt.% based on Table 2, and the LHV was calculated with the correlation reported by Onokwai et al. (2022). The LHV correlation was applied separately to the experimental and to the theoretical HHV, so that the two LHV values differ only through the HHV used. The percentage deviation between experiment and prediction was calculated relative to the experimental value.

$$HHV_{th}\ (MJ/kg) = 0.1905\ VM + 0.2521\ FC \quad (10)$$

$$LHVth\ (MJ/kg) = HHVth - 0.218\ H \quad (11)$$

$$Deviation\ (\%) = \frac{HHV_{exp} - HHV_{th}}{HHV_{exp}} \times 100 \quad (12)$$

where VM and FC are the volatile-matter and fixed-carbon contents (%) and H is the hydrogen content (wt.%). The coefficient 0.218 corresponds to the latent heat of water vapour (about 2.44 MJ/kg) multiplied by the 9 kg of water formed per kg of hydrogen and neglects the smaller correction for moisture.

2.7 X-Ray Diffraction (XRD) Analysis

Wide-angle X-ray diffraction (WAXD) profiles were collected on a Thermo Scientific ARL'XTRA X-ray diffractometer (Serial No. 197492086) utilizing Cu-Kα radiation (λ=1.54060 A˚) operated at 45 kV and 40 mA. Diffraction patterns were recorded across a 2θ range of 5◦ to 60◦ with a step size of 0.05◦ and a scan rate of 1◦C/min at room temperature.

Crystalline phase identification was carried out using integrated system software. Interplanar lattice spacings (d) were calculated via Bragg's Law according to Equation (13):

$$n\lambda=2d\sin\theta \quad (13)$$

where n is an integer order of reflection, λ is the X-ray wavelength, θ is the diffraction angle, and d is the interplanar spacing. The full width at half maximum (FWHM) of characteristic peaks was subsequently utilized to estimate average crystallite size via the Scherrer equation.

2.8 Fourier Transform Infrared Spectroscopy (FTIR)

Functional group characterization was performed via FTIR spectroscopy using a Shimadzu FTIR-8400S spectrophotometer. Powdered samples were evaluated directly using an Attenuated Total Reflectance (ATR) sample stage. Background spectrum acquisition was conducted prior to sample measurements to correct for ambient atmospheric interference. Transmittance spectra were recorded across the mid-infrared region (4000–500 cm^{-1}) at a spectral resolution of 4 cm^{-1}. Observed absorption bands were indexed against reference spectral libraries for functional group identification.

2.9 Scanning Electron Microscopy (SEM) with Energy-Dispersive X-Ray Spectroscopy (EDX)

Surface morphology was evaluated using a Phenom World SEM (Model PRO, Serial No. MVE01570775) operating at an accelerating voltage of 20 kV. Powdered specimens were mounted onto double-sided conductive adhesive carbon tabs and sputter-coated with a 5 nm gold film using a Quorum Technologies Q150R coater to eliminate surface charging. Samples were visually aligned in optical mode prior to switching to electron imaging mode. Micrographs were captured at scale magnifications corresponding to 80 μm and 100 μm. Elemental analysis (weight % and atomic %) was performed concurrently using an integrated Phenom World EDX detector to corroborate crystalline phase distributions identified by XRD.

2.10 Thermal analysis (TGA/DTG and DSC)

Thermogravimetric analysis was performed using a TGA 4000 analyser (PerkinElmer, Netherlands) equipped with an automated data acquisition system. Samples pulverized to <53 μm were heated from ambient conditions (~55°C) to 900°C at a constant heating rate of 10∘C/min under a continuous nitrogen (N_2) atmosphere, with an isothermal hold at 900°C for 10 min. DTG curves were derived from the primary TGA profiles to identify peak mass loss rate temperatures (T_{max}) corresponding to distinct stages of moisture evaporation,

hemicellulose decomposition, cellulose degradation, and lignin thermal breakdown. DSC analysis was conducted using a DuPont 2100 thermal analysis system equipped with standard calorimetric modules. Thermal transitions, including endothermic moisture volatilization, glass transition, hemicellulose softening, and exothermic oxidative breakdown were evaluated for pure and blended samples. DSC thermograms were interpreted alongside TGA/DTG data to quantify enthalpies associated with major thermal events.

3.0 Results and Discussion

The results are presented in the order in which they build the argument: fuel composition (proximate, fibre and elemental), energy content (experimental against theoretical heating values), structure and morphology (XRD, FTIR, SEM-EDX), thermal decomposition (TGA/DTG, DSC), and the resulting implications for blend design. Proximate values are single determinations; differences of a fraction of a percent between neighbouring blends are therefore indicative only.

3.1 Proximate Analysis

Biomass fuels are primarily characterized by four proximate parameters: Moisture Content (MC), Volatile Matter (VM), Ash Content (AC), and Fixed Carbon (FC). These parameters serve as foundational metrics for predicting devolatilization dynamics, calorific yields, and overall combustion behaviour.

Table 2. Proximate analysis of raw biomass and composite briquettes (wt.%, single determination).

Sample	MC	VM	AC	FC (Eqn. 4)	Sum
RH	7.64	56.22	11.24	24.91	100.00
PKS	7.38	70.21	1.37	21.04	100.00
A (90:10)	4.18	74.39	19.32	2.11	100.00
B (80:20)	4.25	77.90	17.34	0.51	100.00
C (70:30)	5.51	78.18	16.08	0.23	100.00
D (60:40)	5.57	81.09	13.29	0.05	100.00
E (50:50)	5.54	81.38	12.48	0.60	100.00

FC = fixed carbon by difference (Equation 4); Sum = MC + VM + AC + FC.

The proximate results are compiled in Table 2. The MC of the raw materials (7.64% for RH; 7.38% for PKS) falls within the acceptable thresholds (<10-15%) for solid biofuels reported in the literature (Martinez, 2021; Acevedo et al., 2018; Alonge & Obayopo, 2023). The composite briquettes showed lower moisture levels (4.18%-5.57%) owing to extended drying. Low moisture promotes easy ignition and minimises parasitic thermal losses during water vaporisation.

Raw RH had a low VM content (56.22%), which typically hinders flame propagation and high-temperature ignition. Incorporating PKS raised the VM of the composites to 74.39%-81.38%. The cassava-starch binder, which is itself rich in volatiles, probably contributes to this increase, since the briquette VM exceeds that of both feedstocks. High volatile content enhances flame reactivity and ignition ease, rendering the composites suitable for domestic cookstoves. Pristine PKS had minimal ash (1.37%), whereas raw RH recorded 11.24% ash, typical of silica-rich agricultural residues. Within the briquettes, increasing the PKS fraction reduced ash from 19.32% (90:10) to 12.48% (50:50). The briquette ash values exceed that of the raw RH powder, which cannot result from mixing alone, but an indication that the fine fraction used for briquetting was enriched in mineral matter (silica and soil-derived Al, Ca and K, as detected by EDX; section 3.7) relative to the bulk raw powder analysed. Lower ash content is desirable as it minimises clinker formation, slagging and furnace corrosion during combustion.

Fixed carbon was obtained by difference (Eqn. 4) and, because MC, VM and AC were determined on the same as-determined basis, the four fractions close to exactly 100.00% for every sample (Table 2). Because FC is a residual, it carries the combined weighing and rounding error of the three measured fractions in these single determinations, and the very small FC values of the briquettes (0.05-2.11%) are therefore indicative rather than precise.

Whereas pristine RH and PKS yielded higher experimental heating values (28.10 MJ/kg and 31.62 MJ/kg, respectively) than typical literature averages (due to dry-basis drying), the composites showed very low fixed carbon (0.05%-2.11%). Among the composite blends, increasing the PKS ratio established a linear upward trend in both HHV (rising from 16.92 MJ/kg to 19.19 MJ/kg) and LHV (rising from 15.25 MJ/kg to 17.29 MJ/kg). Sample E (50RH:50PKS) delivered the highest energy density among all composite briquettes, surpassing typical non-woody biomass briquette values (16.46–18.60 MJ/kg) reported by Akam et al. (2024), Kayode et al. (2021), and Tanko et al. (2020). The low FC of the briquettes, against 21-25% for the raw feedstocks, is mainly a consequence of the high

volatile and ash fractions and indicates that the briquettes are volatile-dominated fuels, because they will ignite readily, but the char-burning phase will be short.

3.2 Lignocellulosic Compositional Analysis

The lignocellulosic compositions (cellulose, hemicellulose, and lignin) of pristine RH and PKS are detailed in Table 3.

Table 3. Lignocellulosic Component Comparison of Raw Biomass

Biomass sample	Cellulose (%)	Hemicellulose (%)	Lignin (%)
Rice husk (RH)	**18.24** (28.5-36.5) *	**29.82** (20.1-31.7) *	**30.06** (18.1-26.2) *
Palm kernel shell (PKS)	**15.91** (20.7-45.7) *	**17.44** (6.4-25.0) *	**58.72** (43.0-53.4) *

*Literature ranges from Onokwai et al. (2022), Nakason et al. (2019), Srinivasan et al. (2024), Gani (2024), Kaniapan et al. (2021), Ninduangdee (2015), Sebastine et al. (2023) and Sreesvarna et al. (2019).

The lignocellulosic compositions (cellulose, hemicellulose and lignin) of pristine RH and PKS are given in Table 3. RH contained more cellulose (18.24%) and more hemicellulose (29.82%) than PKS (15.91% and 17.44%), whereas PKS contained exceptionally high lignin (58.72%), roughly twice that of RH (30.06%). Both feedstocks have cellulose fractions below the literature ranges, and the lignin of both lies above them (PKS 58.72% against 43.0-53.4%; RH 30.06% against 18.1-26.2%). The three fractions together account for 78.1% of RH and 92.1% of PKS; the balance is ash (11.24% and 1.37%) and extractives. Cellulose here is the ADF-ADL difference, so it measures chemical content and says nothing about crystallinity, which is addressed by XRD in section 3.5.

Hemicellulose is the most reactive polymer and explains the rapid early devolatilisation of RH, while lignin, a thermosetting phenylpropanoid network rich in methoxy and phenolic hydroxyl groups, decomposes slowly over a wide temperature range and favours prolonged char oxidation and higher calorific output. Combining the two in the 50:50 ratio therefore couples the volatile-rich RH with the lignin-rich PKS and gives a more balanced thermal decomposition profile (section 3.8).

3.3 Ultimate Analysis

The elemental concentrations (C, H, N, S, and O) of the raw materials and composite briquettes are reported in Table 4

Table 4. Ultimate analysis of raw biomass and composite briquettes (wt.%).

Sample	C	H	N	S	O	Sum
RH	28.86	29.25	0.56	0.80	30.05	89.52
PKS	30.74	15.28	1.06	0.90	40.42	88.40
A (90:10)	42.60	17.43	0.75	1.08	31.08	92.94
B (80:20)	29.70	27.33	0.81	0.87	30.05	88.76
C (70:30)	32.70	16.27	0.67	0.86	47.83	98.33
D (60:40)	30.54	13.58	0.61	0.84	46.30	91.87
E (50:50)	43.62	15.46	0.84	0.83	28.79	89.54

Sum = C + H + N + S + O.

The elemental concentrations are reported in Table 4. Sample E (50RH:50PKS) recorded the highest elemental carbon content (43.62%) and the primary energy-yielding element during complete oxidation, which is consistent with the elevated heating value of sample E. Because the carbon in samples A and E exceeds that of both raw materials, the carbon-rich cassava-starch binder (25% of the briquette mass) is the likely cause, as there is no explanation that can be given for now. Raw RH showed the highest hydrogen content (29.25%), even though this could promote volatile ignition and high flame velocity, its value is too high and cannot be explained at this time. Nevertheless, all composite samples maintained low nitrogen (0.61%-0.84%) and sulphur (0.83%-1.08%) concentrations, indicating a minimal potential for nitrogen oxide (NOx) and sulphur dioxide (SO_2) emissions, which supports clean domestic energy applications.

The hydrogen values (13.58-29.25%) are well above the 4-7% usually found in lignocellulosic biomass as they probably could include hydrogen from residual moisture and hydroxyl groups retained by the hygroscopic powders during the analysis, being an offset that is systematic across all samples and therefore does not alter the relative comparisons between formulations;

although it is accepted that it will propagate into the LHV values in section 3.4 (Eqn. 11), which should be read as lower bounds. Also, the fact that the totals of C, H, N, S and O (88.4-98.3%) fall short of 100% could be because the ash and other inorganic constituents are not part of the CHNSO sum. Further investigations are needed.

3.4 Experimental and Calculated HHV

The theoretical HHV and LHV were derived using empirical models based on proximate and ultimate parameters HHV_{th} (MJ/kg) = 0.1905 VM + 0.2521 FC, LHV_{th} (MJ/kg) = HHV_{th} − 0.218 H

Table 5. Experimental and theoretical heating values (MJ/kg).

Sample	HHV exp.	HHVtheor. (Eqn. 10)	LHVexp.	LHVtheor. (Eqn. 11)
RH	28.10	16.99	21.72	10.61
PKS	31.62	18.68	28.29	15.35
A (90:10)	16.92	14.70	13.12	10.90
B (80:20)	17.99	14.97	12.03	9.01
C (70:30)	18.14	14.95	14.59	11.40
D (60:40)	18.69	15.46	15.73	12.50
E (50:50)	19.19	15.65	15.82	12.28

The experimental HHV of the briquettes rose from 16.92 MJ/kg (A) to 19.19 MJ/kg (E) as the PKS fraction increased (Table 5). Sample E (50RH:50PKS) delivered the highest energy density among all composite briquettes, surpassing typical non-woody biomass briquette values (16.46-18.60 MJ/kg) reported by Akam (2024), Kayode (2021) and Tanko et al. (2020). The theoretical HHV from Eqn. 10 was 14.70-15.65 MJ/kg, so the correlation under-predicted the experimental value by 2.2-3.5 MJ/kg (13-18%), with the largest gap for sample E. The theoretical LHV (9.0-12.5 MJ/kg) is correspondingly lower than the experimental LHV (12.0-15.8 MJ/kg), because both are reduced by the same hydrogen term (0.218 H, about 2.4-6.0

MJ/kg); sample B, with the highest hydrogen of the blends (27.33%), has an LHV below that of A despite its higher HHV.

A hypothesis can be provided for the difference between experimental and theoretical values partly as follows: the briquettes contain 25% cassava-starch binder, a carbohydrate with a high volatile content whose energy is only partly captured by the biomass-based correlation; the calorimeter measures the whole sample including its moisture and ash behaviour, whereas the correlation is not corrected for them; and the fact that the experimental scatter could be quantified because the heating values are single measurements. The unbriquetted RH (28.10 MJ/kg) and PKS (31.62 MJ/kg) powders gave values far above the published ranges for these feedstocks (about 14-18 MJ/kg for RH and 16-22 MJ/kg for PKS) and above the briquettes made from them; these two values were obtained in a separate calorimeter runs and are therefore not used to judge the effect of blending, which is assessed on the briquettes A-E measured under the same conditions.

In conclusion, the experimental calorific values were consistently higher than the theoretical estimations because empirical models based strictly on volatile matter and fixed carbon do not fully capture the synergistic combustion effects between lignin-rich PKS char and starch binder agglomeration. Therefore, sample E (50RH:50PKS) represents the optimal formulation balance for thermal and environmental efficiency resulting from peak carbon content (43.62%), reduced ash fraction (12.48%), and maximum composite HHV (19.19 MJ/kg). Also, a demonstration of economic viability is shown by replacing 50% of PKS with RH as it offers a cost-effective, high-performing solid fuel option for areas where PKS availability is limited or costly.

3.5 X-ray Diffraction (XRD)

X-ray diffraction was used to examine the degree of structural order of RH, PKS and their mixtures. The diffractograms in Figure 3 show a broad diffuse feature centred at approximately $2\theta = 22.01°$ for all samples, consistent with the predominantly disordered character expected for lignocellulosic agricultural residues. Rice husk commonly exhibits a broad halo at about 20-24° 2θ because of the combined contribution of amorphous silica and the less ordered lignocellulosic matrix, and the present maximum lies within the range reported for rice-husk-derived amorphous silica and raw rice husk (Battegazzore et al., 2014; Ong et al., 2021). It should not be assigned exclusively to amorphous SiO_2, because cellulose also contributes broad features in this region. By Bragg's law (Equation 13) the 22.01° maximum corresponds to d = 4.03 Å. A weak shoulder near 16° is visible in some patterns and is typical of cellulose I.

The small variation in the principal 2θ position among RH, PKS and the blends shows that blending did not produce a new crystalline phase; it only changed the relative contribution of the structural components already present in the two feedstocks. This agrees with the established structure of lignocellulosic biomass, in which crystalline cellulose is embedded in an amorphous matrix of hemicellulose, lignin and extractives, plus a substantial inorganic silica fraction in rice husk (Ong et al., 2021). No sharp reflections of quartz, phosphate or other crystalline mineral phases were identified in any pattern, and no phase assignment beyond the amorphous halo is made.

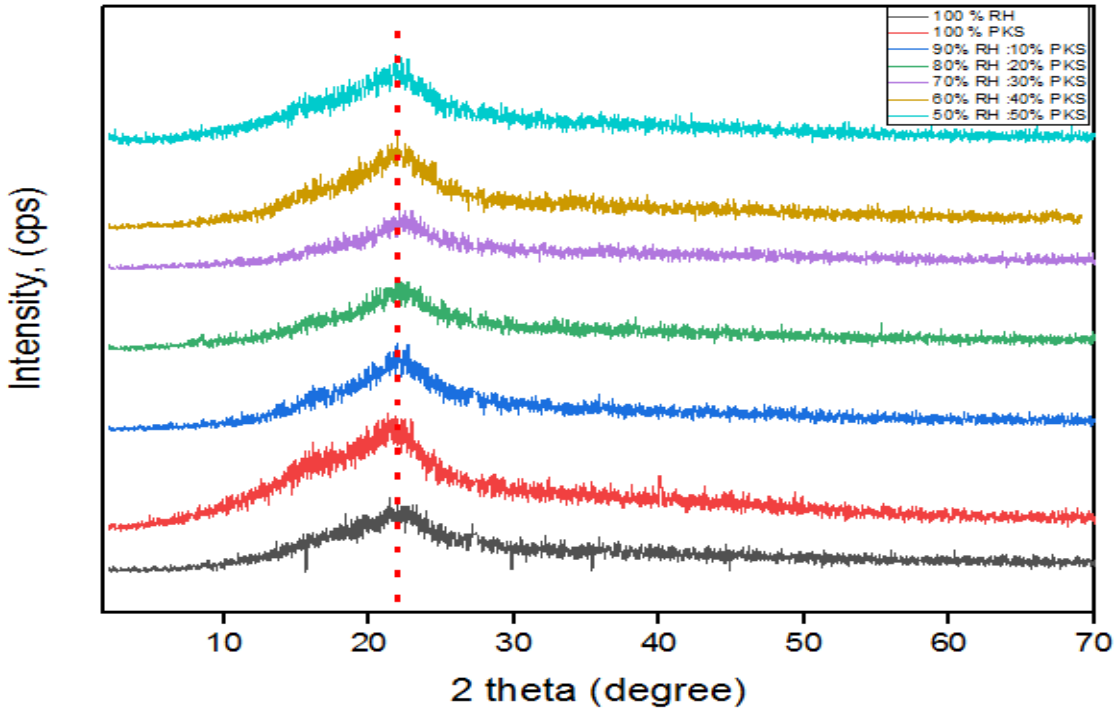


Figure 3. XRD patterns of RH, PKS and their mixtures.

3.6 Fourier Transform Infrared Spectroscopy (FTIR)

The FTIR spectra (Figure 4) provide complementary evidence for the lignocellulosic and mineral constituents inferred from XRD. The assigned bands are listed in Table 6. The broad band at 3324.78 cm^{-1} in PKS is assigned to O-H stretching of hydroxyl groups in cellulose, hemicellulose and lignin, together with adsorbed moisture, in line with PKS hydroxyl bands reported near 3347-3400 cm^{-1} (Ezzuldin et al., 2019; Huang et al., 2018). The bands at 2914.77 cm^{-1} (PKS) and 2922.23 and 2855.14 cm^{-1} (RH) are aliphatic C-H stretches of CH_2/CH_3 groups (Huang et al., 2018; Ong et al., 2021).

Table 6. FTIR band positions and functional-group assignments.

Wavenumber (cm^{-1})	Sample	Assignment
3324.78	PKS	O-H stretching (cellulose, hemicellulose, lignin, adsorbed water)
2922.23 / 2914.77	RH, mixtures A-E / PKS	Aliphatic C-H asymmetric stretching (-CH_2, -CH_3)
2855.14	RH	Aliphatic C-H symmetric stretching
1714.57	PKS	C=O stretching (ester, aldehyde, ketone or carboxylic acid; hemicellulose and lignin)
1647.48	RH, mixtures A-E	Conjugated C=O / aromatic C=C and H-O-H bending of adsorbed water
1595.30	PKS	Aromatic skeletal C=C vibration (lignin)
≈1053	RH	Si-O-Si asymmetric stretching overlapping C-O stretching
1028.74	PKS, mixtures A-D	C-O stretching of cellulose and hemicellulose; may overlap Si-O-Si
782.74	RH	Si-O-Si symmetric stretching (silica)

The bands at 1714.57 and 1595.30 cm^{-1} indicate carbonyl-containing and aromatic/conjugated structures, although a single band cannot distinguish carboxyl, imine or azo groups; this is as evidence of carbonyl functionality. The band at 1647.48 cm^{-1} in RH may combine conjugated carbonyl/aromatic vibrations with the deformation of adsorbed water. The 1000-1100 cm^{-1} region is the strongest evidence of the lignocellulosic framework; in RH it is a superposition of C-O/C-O-C vibrations of the carbohydrates and Si-O-Si vibrations of silica, consistent with the observation of intense rice-husk silica bands near 1047 and 800 cm^{-1} (Battegazzore et al., 2014; Ong et al., 2021) and in agreement with the broad XRD halo near 22°. Hydroxyl functionality is an established feature of lignocellulosic biomass and rice-husk-derived silica (Battegazzore et al., 2014).

The superimposed spectra show that RH and PKS share the main regions expected for lignocellulosic materials but differ in relative band intensity: RH shows stronger absorption at 1000-1200 cm^{-1} (silica-rich), whereas PKS shows features associated with lignin and aliphatic structures; PKS lignin is of the H-G-S type with abundant β-O-4 linkages (Huang et al., 2018). In the mixtures the 1647.48 and 2922.23 cm^{-1} bands persist (A-E) and the 1028.74 cm^{-1} band is resolved in PKS and most blends except E, whereas the RH bands at 2855.14 and 782.74 cm^{-1} are not resolved. These changes are consistent with dilution, band overlap and a change in the relative abundance of the components, and not with new chemical species. Overall, the FTIR results validate the presence of the principal chemical building blocks of lignocellulosic biomass—cellulose, hemicellulose and lignin—together with the silica-rich mineral fraction characteristic of RH, and with the XRD evidence of a predominantly disordered material (Battegazzore et al., 2014; Ong et al., 2021).

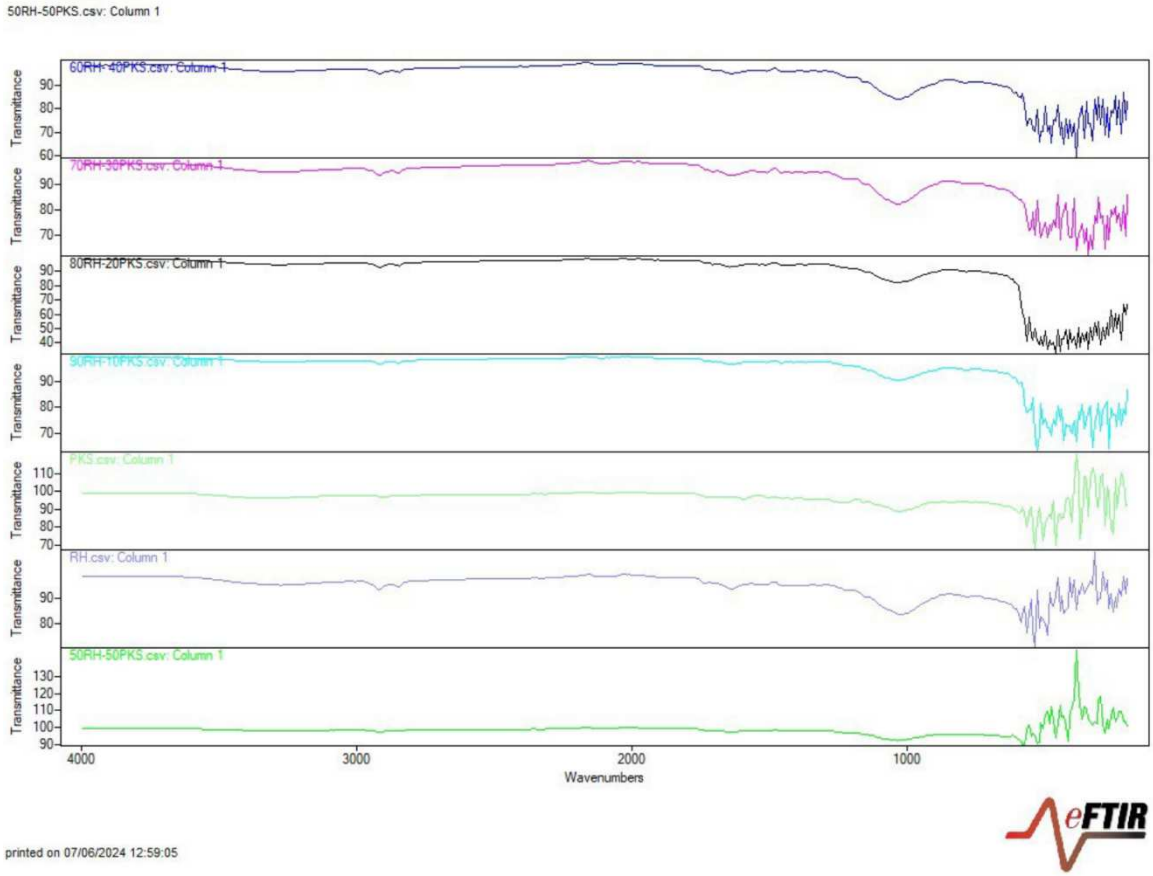


Figure 4. Superimposed FTIR spectra of the different compositions.

3.7 Scanning Electron Microscopy (SEM) and Energy-Dispersive X-ray (EDX) Analysis

SEM micrographs (500×, 15 kV) were combined with EDX analysis to relate surface morphology to composition (Figure 5). The RH micrograph shows a fibrous, heterogeneous

surface with pores, irregular features and cracks, consistent with the anatomy of rice husk, whose outer epidermis contains ridges, lignified structures and concentrated silica deposits (Park et al., 2003). The EDX spectrum of RH identifies carbon, silicon and nitrogen as principal elements, with phosphorus, magnesium, potassium, aluminium, calcium and other minor elements. The PKS micrograph shows a relatively compact, closely packed surface, in line with SEM observations of raw PKS (Ezzuldin et al., 2019); PKS particles can therefore contribute dense packing in a blend, and PKS-derived materials compact effectively when moisture, pressure and curing are suitable (Bazargan et al., 2014).

The 90:10 mixture shows the porous, irregular morphology of RH; with increasing PKS content the cracks and surface roughness decrease and compactness increases, reflecting the different particle geometry and packing of the two feedstocks. The EDX results indicate carbon, silicon and nitrogen as dominant detected elements in the mixtures, with P, Mg, K, Al, Na, Fe, Ca, Cl, S and Ti at lower levels, as expected from mineral nutrients and soil-derived matter in agricultural residues. EDX is surface-sensitive and semi-quantitative, and its values for light elements such as nitrogen should not be taken as bulk composition. Together, XRD, FTIR and SEM-EDX describe a heterogeneous, predominantly disordered lignocellulosic material: XRD gives its structural order, FTIR its functional groups and silica contribution in RH, and SEM-EDX its morphology and near-surface elements.

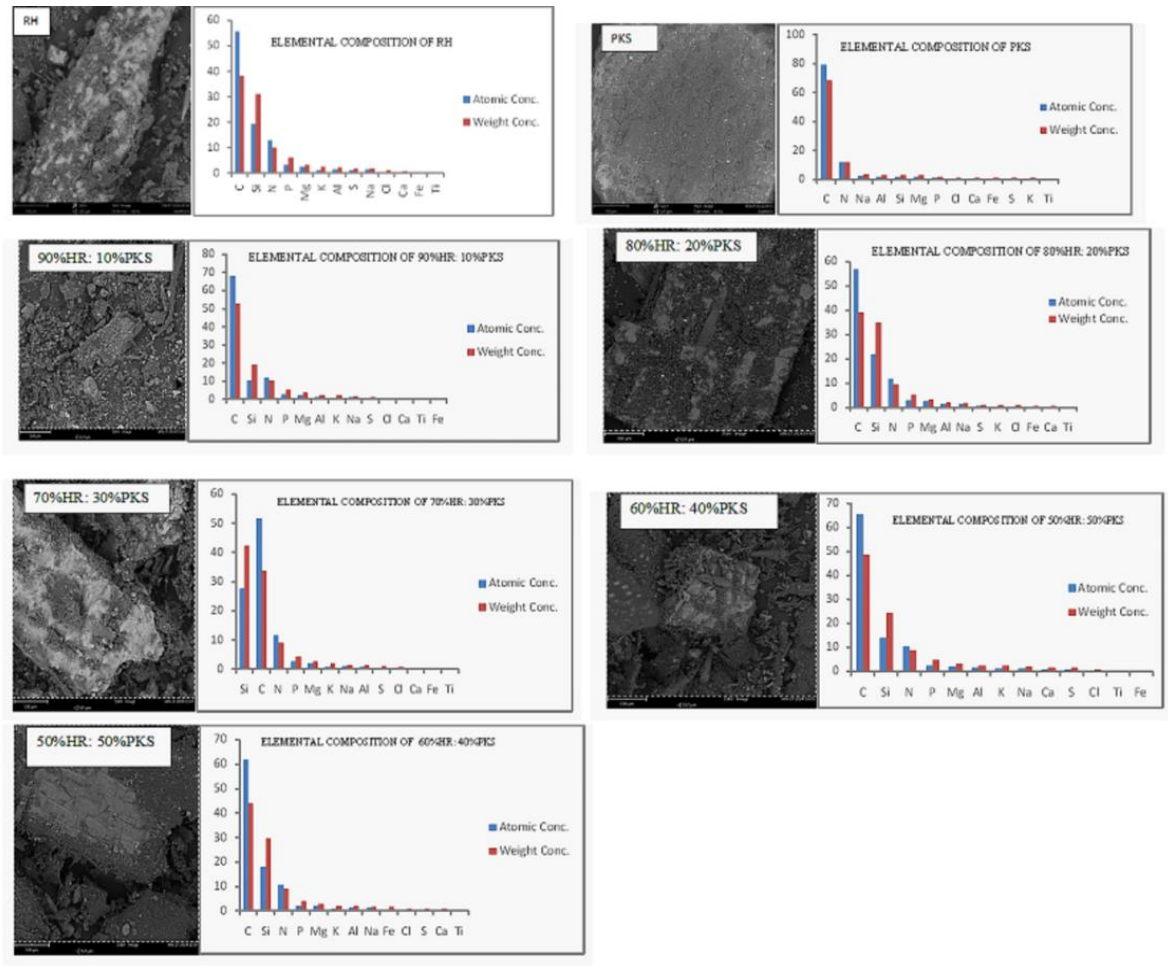


Figure 5. SEM micrographs and EDX spectra of RH, PKS and their mixtures.

3.8 Thermogravimetric Analysis (TGA)

The composite TGA and DTG curves are shown in Figures 6. RH exhibited three principal degradation zones, consistent with the pattern widely reported for lignocellulosic biomass (Ngoc et al., 2018; Azat et al., 2019; Adhityatama et al., 2017; Glushankova et al., 2018; Nayak & Datta, 2022). The first zone, beginning at approximately 300 °C, corresponds to the major devolatilisation of hemicellulose together with part of the cellulose, with an initial mass loss of 28%. The third zone, at 460 °C, represents the continuing degradation of lignin, where the highest overall mass loss occurred. These temperatures agree with the literature, which places hemicellulose decomposition below about 400 °C and lignin decomposition as a slow, wide process extending well beyond it because of lignin's aromatic, cross-linked structure (Azat et al., 2019). Unlike several cited studies, no distinct surface-moisture loss event was observed in the 105-166 °C region for RH, in contrast with the discrete dehydration stage at 30-166 °C

reported by Ngoc et al. (2018); this may reflect the moisture content at the time of testing, sample pre-drying or instrument sensitivity.

PKS degraded in as many as six distinguishable zones, a multi-zone pattern comparable with that reported by Kaniapan et al. (2021). The maximum mass losses, 36% and 41.5% in the second and fourth zones, correspond approximately to near-complete hemicellulose degradation extending into cellulose degradation (Adhityatama et al., 2017). The fifth and sixth zones, at 550 °C and 680 °C, indicate lignin far advanced in decomposition alongside residual cellulose; the sixth-zone temperature exceeds the third-zone temperature of RH, consistent with the higher lignin content of PKS (Table 4). Lignin decomposition may continue beyond 680 °C (Kaniapan et al., 2021; Hamza et al., 2016), and the hemicellulose window observed here (about 240-318 °C) agrees with the literature.

The blends each showed three degradation zones, with the third (lignin) zone shifting to higher temperature as the PKS fraction increased, a direct consequence of the higher lignin content of PKS. A plateau in this third zone, and in the first zone, was observed for the lignin-richer blends (70:30 to 50:50), and the second zone rose systematically with PKS content. Within 90:10-50:50 the mixing ratio therefore shifts degradation temperature approximately linearly, and the effect saturates once lignin-dominated behaviour prevails.

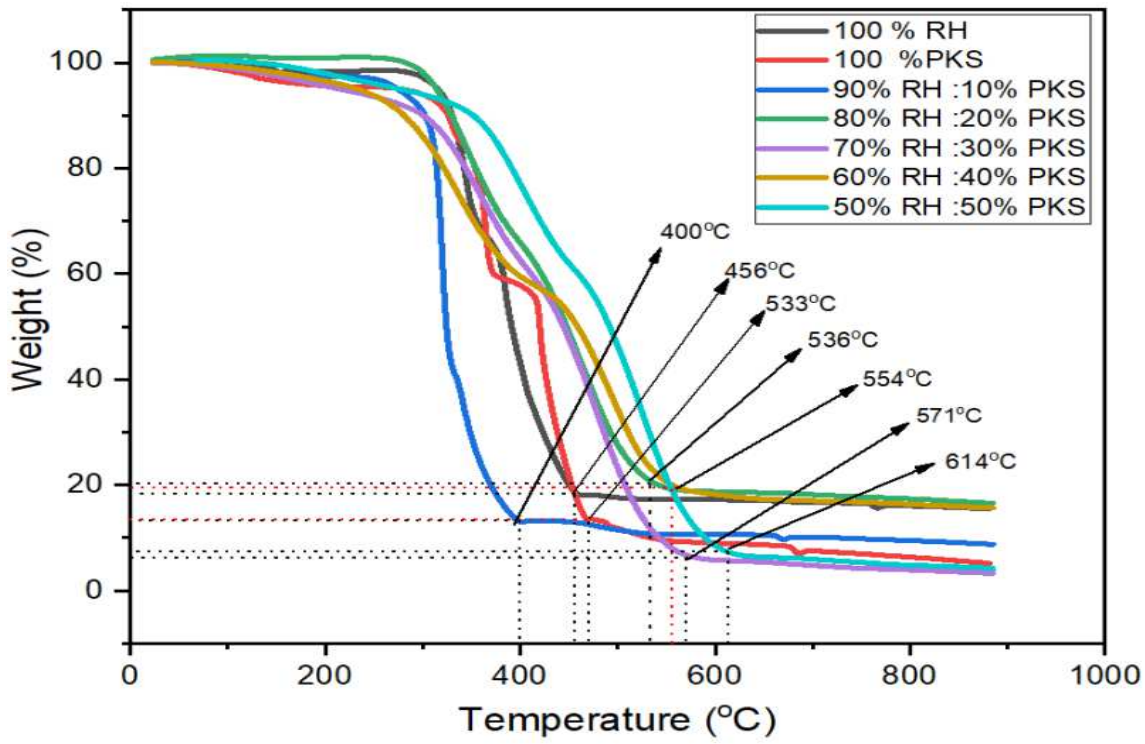


Figure 6. TGA of RH, PKS and their compositions.

3.9 Differential Thermal Gravimetry (DTG)

The DTG curves (Figure 7) all show a main mass-loss region between about 250 and 600 °C with a weak shoulder near 300 °C. Read from the figure, the maximum rate occurs at approximately 330 °C for 90:10 (the sharpest peak, about -12 %/°C), at approximately 380-390 °C for RH and PKS, and between about 440 and 480 °C for the 80:20 to 50:50 blends, with lower and broader peaks. A small broad feature near 120-125 °C for 90:10 is attributed to surface and embedded moisture. The 90:10 peak is much sharper than that of pure RH, which may reflect the more rapid, concerted devolatilisation of the finer, volatile-rich fraction in this blend. These features agree with the literature for RH: Azat et al. (2019) reported hemicellulose and cellulose loss at 210-360 °C with a DTG peak at 330-360 °C and gradual lignin loss from about 380 °C to 600-800 °C; Ngoc et al. (2018) reported dehydration at 30-166 °C (6.7%), a major stage at 166-405 °C (54.0%) and a third stage at 405-900 °C (20.1%), with a total mass loss of 80.9%; and El-Sayed (2019) reported DTG peaks at 53.6, 211.3, 300 and 469 °C. Regional variability in RH thermal behaviour (variety, soil, climate) implies that each supply batch should be characterised.

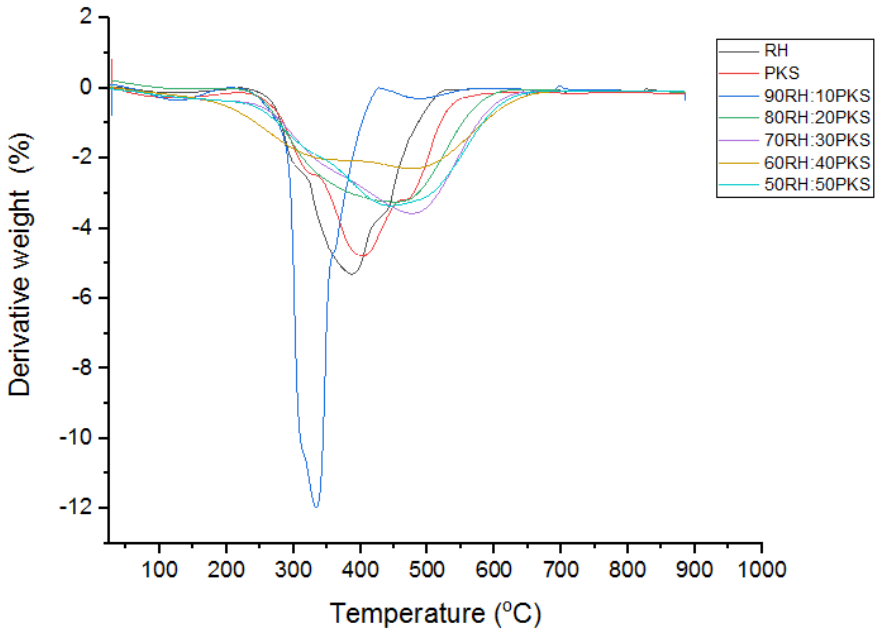


Figure 7. DTG of RH, PKS and their compositions.

3.10 Differential Scanning Calorimetry (DSC)

The composite DSC plot (Figure 8) shows similar patterns for RH and PKS up to approximately 300 °C, diverging from about 260 °C. Both materials show two major heat-flow minima in the regions of about 62-85 °C and 140-152 °C for RH, against about 100-124 °C for PKS, attributable to evaporation of surface water, an endothermic process. Around 260 °C, PKS shows a broad exothermic peak that may point to a crystallisation-related process in the cellulose fraction. RH shows smaller peaks near 210 °C, which may reflect oxidation and decomposition, potentially of carboxylic groups in the cellulose/hemicellulose fraction, together with loss of embedded water. No consistent degradation of peak temperature with increasing PKS content was observed.

Most of the cited DSC literature reports data beyond 300 °C (Nayak & Datta, 2022; Ntenga, 2018; Dhaneswara et al., 2019; Baffour-Awuah, 2021; Djomi, 2018), and several of these studies report peaks across a wide 110-300 °C window, which underscores the variability of biomass thermal properties with feedstock, origin and pretreatment and supports characterising each batch of RH and PKS. The moisture-loss events below about 150 °C reflect why briquettes must be adequately dried before use: energy that would drive combustion is consumed in evaporating residual moisture, lowering effective heat output and increasing smoke during ignition. The absence of a systematic shift with blend ratio is a useful result for design, since

blending can tune burn duration and char yield (Section 3.8) without changing low temperature drying and ignition behaviour.

Taken together, the results show RH and PKS to be complementary rather than interchangeable feedstocks. RH contributes hemicellulose and volatile matter, a simple three-zone decomposition at lower temperature, and therefore rapid ignition and volatile release, which suits quick-boil cooking. PKS contributes lignin (58.72%), low ash and a multi-zone, higher-temperature decomposition with a longer char-burning tail, which suits sustained simmering and space heating. Across the 90:10-50:50 range the degradation temperature rises approximately linearly with PKS content before saturating, and the experimental HHV rises from 16.92 to 19.19 MJ/kg while the ash falls from 19.32% to 12.48%. Sample E (50RH:50PKS) therefore combines the highest heating value, the lowest briquette ash and the highest carbon content, and offers a hot start followed by sustained heat without chemical additives. Replacing half of the PKS with the more readily available RH also offers an economic route where PKS is limited or costly. These conclusions are based on single determinations and on an exploratory thermal dataset.

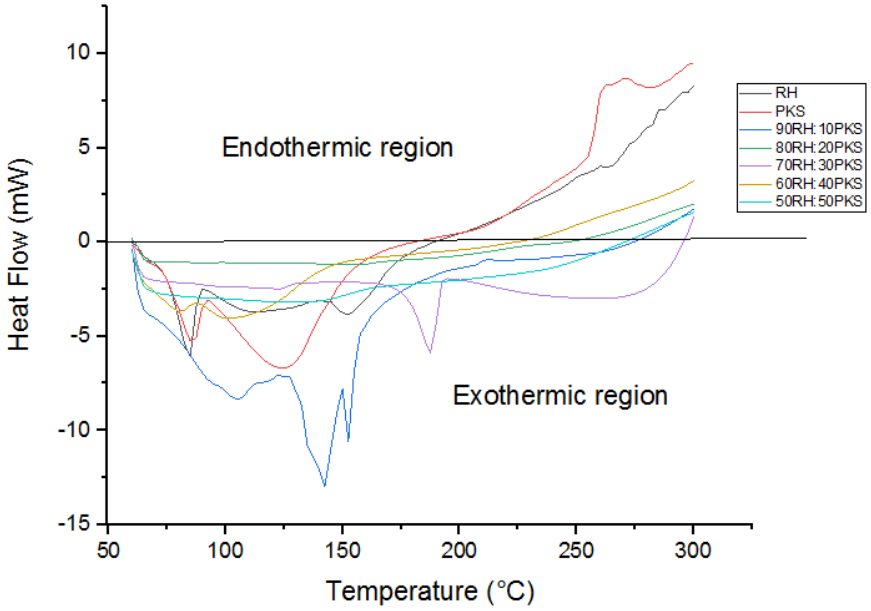


Figure 8. DSC of RH, PKS and their compositions.

4. Conclusions and outlook

RH-PKS blends were evaluated as a fuel-design option rather than a proven household fuel. Increasing the PKS fraction lowered ash (19.32% to 12.48%), raised volatile matter (74.39%

to 81.38%) and raised the experimental HHV from 16.92 to 19.19 MJ/kg, with sample E (50:50) the best of the blends. PKS supplied lignin (58.72%) and RH hemicellulose (29.82%). XRD and FTIR showed an amorphous lignocellulosic matrix with silica-related features in RH, SEM-EDX showed a transition from the porous RH morphology to the compact PKS morphology as PKS increased, and TGA/DTG showed that RH-rich samples decompose at lower temperature than PKS-rich blends, so that the RH:PKS ratio can balance early volatile release against sustained heat. The proximate-based HHV correlation under-predicted the measured HHV by 13-18%, and the hydrogen, raw-powder heating-value and briquette ash results should be treated as indicative as further work is necessary. The absence of a systematic shift with blend ratio in the DSC portends a useful result for design, as it points to the fact that blending can tune burn duration and char yield without changing low temperature drying and ignition behaviour. Sample E (50RH:50PKS) combines the highest heating value, the lowest briquette ash and the highest carbon content, offering a hot start followed by sustained heat. Replacing half of the PKS with the more readily available RH, similarly offers an economic route where PKS is limited or costly. Moreover, the fact that all composite samples maintained low nitrogen (0.61%-0.84%) and sulphur (0.83%-1.08%) concentrations, is evidence of a minimal potential for nitrogen oxide (NOx) and sulphur dioxide (SO_2) emissions and supports clean domestic energy applications. These conclusions, although based on single determinations and on an exploratory study of thermal dataset, suggest the potential for some of these blends to be used in domestic cooking and heating on further analyses.

Acknowledgement

The authors wish to acknowledge the financial support from the Tertiary Education Trust Fund (TETFund) through grant no. ref: TETF/ES/DR&D-CE/NRF/2021/SETI/PAE/00012/VOL.1.

Credit authorship contribution statement

UA: Conceptualization, Methodology, Writing - original draft, Writing - review & editing, Resources. **HIJ:** Visualization, Writing - review & editing. **BYA:** Visualization, Writing - review & editing **ASY:** Visualization, Writing - review & editing. **MA:** Visualization, Writing - review & editing. **BA:** Visualization, Writing - review & editing.

Funding

The study was funded by the Tertiary Education Trust Fund (Tetfund) through grant no. ref: TETF/ES/DR&D-CE/NRF/2021/SETI/PAE/00012/VOL.1.

Declaration of Competing Interest

The authors declare that they have no known competing financial interests or personal relationships that could have influenced the work presented in this study.

Data Availability

The data supporting the findings of this study will be made available upon reasonable request.

Declarations

Ethics approval and consent to participate

Not applicable.

Consent for publication

Not applicable.

Competing interests

The authors declare no competing interests

Clinical trial registration

Not applicable. This study does not involve a clinical trial.

References

Acevedo, J. C., Posso, F. R., Durán, J. M., & Arenas, E. (2018). Simulation of the gasification process of palm kernel shell using Aspen PLUS. Journal of Physics: Conference Series, 1126, 012010.

Adhityatama, G. I., Hanif, F., Cahyono, R. B., Hidayat, M., & Akiyama, T. (2017). A comparative study on pyrolysis characteristic Indonesia biomassa and low-grade coal. IOP Conference Series: Earth and Environmental Science, 65, 012001.

Akam, N. G. (2024). Physicochemical characterization of briquette fuel produced from cocoa pod husk case of Cameroon. Energy Reports, 1580-1589.

Alonge, O. I., & Obayopo, S. O. (2023). Optimization study on carbonization of palm kernel shell using response surface method. International Journal of Integrated Engineering, 15, 135-144.

ASTM International. (2019). ASTM D5865/D5865M-19, Standard test method for gross calorific value of coal and coke. ASTM International.

ASTM International. (2021a). ASTM D3172-13(2021)e1, Standard practice for proximate analysis of coal and coke. ASTM International.

Azat, S., Korobeinyk, A. V., Moustakas, K., & Inglezakis, V. J. (2019). Sustainable production of pure silica from rice husk waste in Kazakhstan. Journal of Cleaner Production, 217, 352-359.

Baffour-Awuah, E. (2021). Characteristics of palm kernel shell and palm kernel shell-polymer composites: a review. IOP Conference Series: Materials Science and Engineering, 1107, 012090.

Basu, P. (2013). Biomass gasification, pyrolysis and torrefaction: Practical design and theory (2nd ed.). Academic Press.

Battegazzore, D., Bocchini, S., Alongi, J., & Frache, A. (2014). Rice husk as bio-source of silica: Preparation and characterization of PLA-silica bio-composites. RSC Advances, 4, 54703-54712. https://doi.org/10.1039/C4RA05991C

Bazargan, A., Rough, S. L., & McKay, G. (2014). Compaction of palm kernel shell biochars for application as solid fuel. Biomass and Bioenergy, 70, 489-497. https://doi.org/10.1016/j.biombioe.2014.08.015

Dhaneswara, D., Fatriansyah, J. F., Wardana, A. K., Haqoh, A. N., & Khairunnisa, S. A. (2019). The study of thermal decomposition of rice husk in silica production: the effect of hydrochloric acid leaching. IOP Conference Series: Materials Science and Engineering, 547, 012032.

Djomi, R. (2018). Physicochemical and thermal characterization of Dura palm kernel powder as a load for polymers: case of polyvinyl chloride. Journal of Materials Science and Chemical Engineering, 6, 1-18.

El-Sayed, S. (2019). Thermal decomposition, kinetics and combustion parameters determination for two different sizes of rice husk using TGA. Engineering in Agriculture, Environment and Food, 12(4), 460-469.

Ezzuldin, S. S. M., Abd Rahim, S. B., Wan Yussof, H., Olalere, O. A., & Habeeb, O. A. (2019). Morphological, thermal stability and textural elucidation of raw and activated palm kernel shell and their potential use as environmental-friendly adsorbent. Chemical Data Collections, 21, 100235. https://doi.org/10.1016/j.cdc.2019.100235

Gani, A. (2024). Comparative analysis of HHV and LHV values of biocoke fuel from palm oil mill solid waste. Case Studies in Chemical and Environmental Engineering, 9, 100581.

Glushankova, I., Ketov, A., Krasnovskikh, M., Rudakova, L., & Vaisman, I. (2018). Rice hulls as a renewable complex material resource. Resources, 7, 31.

Hamza, U. D., Nasri, N. S., Amin, N. S., Mohammed, J., & Zain, H. M. (2016). Characteristics of oil palm shell biochar and activated carbon prepared at different carbonization times. Desalination and Water Treatment, 57(17), 7999-8006. https://doi.org/10.1080/19443994.2015.1042068

Huang, Y., Liu, H., Yuan, H., Zhan, H., Zhuang, X., Yuan, S., Yin, X., & Wu, C. (2018). Relevance between chemical structure and pyrolysis behavior of palm kernel shell lignin. Science of the Total Environment, 633, 785-795. https://doi.org/10.1016/j.scitotenv.2018.03.238

Jume, H. I., Alhaji, B. Y., Ahmadu, U., Ibrahim, S. O., Agida, M., Muazu, A., Ndamitso, M. M., & Abdulkadir, B. (2024). Production of briquettes from a blend of rice husks and palm kernel shells as an alternative solid fuel. FUDMA Journal of Sciences, 8(3).

Kaniapan, S., Suhaimi, H., Hamdan, Y., & Pasupuleti, J. (2021). Experiment analysis on the characteristic of empty fruit bunch, palm kernel shell, coconut shell, and rice husk for biomass boiler fuel. Journal of Mechanical Engineering and Sciences, 15, 8300-8309.

Kayode, B. I. (2021). Preparation and characterization of rice and wheat husks composite briquette use as alternative fuel for domestic cooking (Doctoral dissertation).

Lichinga, K. N., Sikazwe, K., Elibariki, R., & Shija, H. (2025). Cleaner cooking solutions: Optimizing biomass briquettes to replace charcoal. Scientific African, 18, e01345.

Martinez, A. (2021). Comparative study of the reaction kinetics of three residual biomasses.

Mertens, D. R. (2002). Gravimetric determination of amylase-treated neutral detergent fiber in feeds with refluxing in beakers or crucibles: Collaborative study. Journal of AOAC International, 85(6), 1217-1240.

Möller, J. (2009). Gravimetric determination of acid detergent fiber and lignin in feed: Interlaboratory study. Journal of AOAC International, 92(1), 74-90. https://doi.org/10.1093/jaoac/92.1.74

Nakason, K., Pathomrotsakun, J., Kraithong, W., Khemthong, P., & Panyapinyopol, B. (2019). Torrefaction of agricultural wastes: influence of lignocellulosic types and treatment temperature on fuel properties of biochar. International Energy Journal, 19.

National Bureau of Statistics (NBS). (2024). Nigeria Residential Energy Demand-Side Survey (NREDSS) 2024. National Bureau of Statistics, Abuja, Nigeria.

Nayak, P. P., & Datta, A. K. (2022). An entropy-based TOPSIS approach for selecting best suitable rice husk for potential energy applications: pyrolysis kinetics and characterization of rice husk and rice husk ash. Biomass Conversion and Biorefinery. https://doi.org/10.1007/s13399-022-02824-3

Nigerian Conservation Foundation (NCF). (2026, March 22). NCF raises the alarm over deforestation, says Nigeria lost 90 percent of forest cover in 30 years. AllAfrica. https://allafrica.com/stories/202603230071.html

Ngoc, N. N., Thanh, L. X., Vinh, L. T., & Van Anh, B. T. (2018). High-purity amorphous silica from rice husk: Preparation and characterization. Vietnam Journal of Chemistry, 56, 730-736.

Ninduangdee, P. (2015). Thermogravimetric studies of oil palm empty fruit bunch and palm kernel shell: TG/DTG analysis and modeling. Energy Procedia, 79, 453-458.

Ntenga, R. (2018). Insight on the ultrastructure, physicochemical, thermal characteristics and applications of palm kernel shells. Materials Sciences and Applications, 9, 790-811.

Ong, H. C., Yu, K. L., Chen, W. H., Pillejera, M. K., Bi, X., Tran, K.-Q., Pétrissans, A., & Pétrissans, M. (2021). Variation of lignocellulosic biomass structure from torrefaction: A critical review. Renewable and Sustainable Energy Reviews, 152, 111698. https://doi.org/10.1016/j.rser.2021.111698

Onokwai, A. O., Ajisegiri, E. S., Okokpujie, I. P., Ibikunle, R. A., Oki, M., & Dirisu, J. O. (2022). Characterization of lignocellulose biomass based on proximate, ultimate, structural composition, and thermal analysis. Materials Today, 2156-2162.

Park, B.-D., Wi, S. G., Lee, K. H., Singh, A. P., Yoon, T.-H., & Kim, Y. S. (2003). Characterization of anatomical features and silica distribution in rice husk using microscopic and micro-analytical techniques. Biomass and Bioenergy, 25(3), 319-327. https://doi.org/10.1016/S0961-9534(03)00014-X

Qian, C., Li, Q., Zhang, Z., Wang, X., Hu, J., & Cao, W. (2020). Prediction of higher heating values of biochar from proximate and ultimate analysis. Fuel, 265, 116925.

Sebastine, A. B., Michael, A., & Kumaden, I. (2023). Evaluation of the combustion characteristics of rice husk and coconut shell briquettes. Journal of Engineering Research and Reports, 25, 1-9.

Sreesvarna, B., Pugalendhi, S., Subramanian, P., & Gitanjali, J. (2019). Characterization of rice husk for sustainable applications. Madras Agricultural Journal, 106.

Srinivasan, G. R., Mahajan, A., Seth, R., & Mahajan, R. (2024). High potential organic feedstocks for production of renewable solid briquettes: A comprehensive review. Waste Management in the Circular Economy, 231-277.

Tanko, J. U., Sadiq, U., & Muazu, A. (2020). Characterization of rice husk and coconut shell briquette as an alternative solid fuel. Advanced Energy Conversion Materials, 1-12.

Tarigan, E. R., Rahmansyah, A. A., & Khatami, M. (2026). Thermal characterization and heat conductivity of palm kernel shell-based briquettes. Jurnal Presipitasi, 23(2), 572-589.

United Nations. (2015a). Paris Agreement. United Nations Framework Convention on Climate Change, Paris.

United Nations. (2015b). Sustainable Development Goal 7: Ensure access to affordable, reliable, sustainable and modern energy for all. United Nations, New York.

Van Soest, P. J., Robertson, J. B., & Lewis, B. A. (1991). Methods for dietary fiber, neutral detergent fiber, and nonstarch polysaccharides in relation to animal nutrition. Journal of Dairy Science, 74(10), 3583-3597.

Vui, C. K., Jamil, N. H., Che Pa, F., Arif, W. M., Lim, M., Abdullah, M. M. A. B., Zaki, R. M., & Abdullah, H. Z. (2025). Silica extraction from rice husk: A review on the effect of combustion temperature. Archives of Metallurgy and Materials, 70(3), 1473-1478.

World Health Organization (WHO). (2025). Household air pollution and health. Fact sheet. World Health Organization, Geneva.